Statistical Analysis of Contrail to Cirrus Evolution during the Contrail and Cirrus Experiments (CONCERT)

Aurélien Chauvigné[1], Olivier Jourdan[1], Alfons Schwarzenboeck[1], Christophe Gourbeyre[1], Jean François Gayet[1], Christiane Voigt[2,3], Hans Schlager[2], Stefan Kaufmann[2], Stephan Borrmann[3,4], Sergej Molleker[3,4], Andreas Minikin[2,5], Tina Jurkat[2], Ulrich Schumann[2]

[1]Laboratoire de Météorologie Physique, UMR 6016 CNRS/Université Clermont Auvergne, Clermont-Ferrand, France.
[2]Institut für Physik der Atmosphäre, Deutsches Zentrum für Luft- und Raumfahrt (DLR), Oberpfaffenhofen, Germany.
[3]Institut für Physik der Atmosphäre, Universität Mainz, Mainz, Germany.
[4]Max-Planck-Institute for Chemistry, Department for Particle Chemistry, Mainz, Germany.
[5]Now at: Flugexperimente, Deutsches Zentrum für Luft- und Raumfahrt (DLR), Oberpfaffenhofen, Germany.

Abstract:

Air traffic affects the cloudiness, and thus the climate, by emitting exhaust gases and particles. The study of the evolution of contrail properties is very challenging due to the complex interplay of vortex dynamics and atmospheric environment (e.g. temperature, supersaturation). Despite substantial progress in recent years, the optical, microphysical, and macrophysical properties of contrails and ambient cirrus during contrail formation and subsequent ageing are still subject to large uncertainties due to instrumental and observational limitations and the large number of variables influencing the contrail life cycle. In this study, various contrail cases corresponding to different aircraft types and atmospheric conditions are investigated using a statistical method based on the in situ optical measurements performed during the CONCERT campaigns 2008 and 2011. These two aircraft campaigns encompass more than 17 aircraft contrail cases. A Principal Component Analysis (PCA) of the angular scattering coefficients measured by the Polar Nephelometer is implemented. The goal is to classify the sampled ice cloud measurements in 6 clusters representative of different contrail development stages (primary wake, young contrail, contrail-cirrus and natural cirrus). Extinction and, asymmetry coefficients, nitrogen oxide concentrations, relative humidity with respect to ice (RHI) and particle size distributions are analysed for each cluster to characterize the evolution of ice-cloud properties during the contrail to cirrus evolution. The PCA demonstrates that contrail optical properties are well suited to identify and discriminate the different contrail growth stages and to characterize the evolution of contrail properties.

1 Introduction

Aircraft exhaust plumes have a significant impact on climate and tropospheric chemistry (Lee et al., 2010; IPCC, 1999). The Intergovernmental Panel for Climate Change IPCC special report on aviation (1999) estimates that NO_x emissions from subsonic aircraft increase ozone concentrations at cruise level. Short and long lived pollution species have different impact on atmospheric chemical composition depending on the flight level (Frömming et al, 2012). Emissions of water vapour, black carbon (BC) / soot particles, sulphate (SO_4) aerosols and nitrogen oxides (NO_x) contribute to the modification of the chemical composition of the upper troposphere on shorter timescales (Lee et al., 2010, Gettelman and Chen, 2013; Liou et al., 2013). The long-term climate impact is mainly driven by CO_2 emissions. Modelling studies have shown that the direct radiative forcing from aviation is expected to represent 3-4% (50-60 mW m^{-2}) of the anthropogenic forcing (Lee et al., 2010; De Leon et al., 2012) and could reach 87 mW m^{-2} in 2025 (Chen and Gettelman, 2016). Aircraft induced cloudiness has also an important impact on climate, although the quantitative assessment of the radiative forcing remains a major source of uncertainties (Lee et al., 2010).

1.1. Contrail formation and evolution

Contrail formation is mainly controlled by the thermodynamic properties of the ambient air and by the aircraft emissions. The conditions for contrail formation can be determined by the Schmidt-Appleman Criterion (SAC) (Schumann, 1996). Contrail chemical composition can have a significant impact on the contrail formation (Kärcher et al., 2009). Indeed, the contrail microphysical properties, as the total number densities and ice crystal diameters, are directly linked to the emission index (e.g. soot emission index in kg-$fuel^{-1}$). Several studies in the past have been dedicated to the evolution of concentrations of nitrogen oxide (NO) and sulphur dioxide (SO_2) and their oxidized forms (Kärcher and Voigt, 2006 ; Voigt et al., 2006 ; Schäuble et al., 2009 ; Jurkat et al., 2011).

Two different processes of contrail formation have been studied: combustion condensation trails and aerodynamic condensation trails. Different studies (Gierens and Dilger, 2013; Jansen and Heymsfield, 2015) have illustrated characteristics of aerodynamically controlled contrail formation associated to warmer temperatures (observations at temperatures above -38°C). Contrails primarily initiated by the combustion processes result from the mixing of hot and humid exhaust gases with cooler and dryer ambient air. This increases the local relative humidity in the exhaust plume leading to the formation of contrails when the saturation with respect to liquid water is reached. In this case, soot and sulphate aerosols emitted by the aircraft (Moore et al., 2017) may act as condensation nuclei to form liquid droplets. Homogeneous ice nucleation of the liquid droplets can occur when the exhaust cools down through mixing with the ambient temperature, while preserving ice saturation. Small ice crystals are then formed in the jet phase within some tenths of a second (Kaercher and Yu, 2009).

The life-cycle of contrails depends on the interaction with the wake vortices behind aircraft and the ambient atmosphere (Irvine et al., 2012; Graf et al., 2012; Duda et al., 2013; Carleton et al., 2013; Schumann and Heymsfield, 2017). The ice crystals in the young contrails are captured within two counter-rotating wake vortices in the downwash behind the aircraft induced by the aircraft lift, which induce adiabatic compression, heating, and partial sublimation of the ice crystals within the primary wake (Lewellen and Lewellen, 2001; Sussmann and Gierens, 2001, Unterstrasser et al., 2008, Unterstrasser et al., 2016; Kärcher and Voigt, 2017). This primary wake may soon disappear if ambient air is subsaturated with respect to ice. In the case of supersaturation, the secondary wake becomes visible, thereby detraining ice particles from the primary wake at a higher level (Sussmann and Gierens, 1999, Kaufmann et al., 2014). Quasi spherical ice crystals become increasingly aspherical and grow by uptake of water vapour as long as saturation with respect to ice is prevailing. Inice saturated conditions, contrails can persist after the vortex breakdown, spread and evolve into contrail cirrus (Schumann and Heymsfield, 2017). The associated cloud cover (larger than for linear contrails alone) increases thes radiative forcing of contrail cirrus (Burkhardt and Kärcher, 2011; Schumann et al., 2015).

1.2. Optical and microphysical properties of contrail phases

The assessment of the contrail radiative forcing requires, in particular, an accurate estimation of the cloud cover, the visible optical depth, the single scattering characteristics, the ice crystal effective size and habit (Yang et al., 2010; Spangenberg et al., 2013). Satellite observations provide a comprehensive dataset to study statistically the contrail to cirrus evolution. The combined contrail tracking algorithms on the Spinning Enhanced Visible and Infrared Imager (SEVIRI) on board the Meteosat Second Generation (MSG) satellites with properties inferred by the Moderate Imaging Spectroradiometer (MODIS) on board the Terra satellite was used by Vazquez-Navarro et al., (2015) to characterize the properties of 2300 contrails. Properties included lifetime (mean values of 1h), the length (130 km), the optical thickness (0.34), the altitude (11.7 km) and the radiative forcing (-26 W m^{-2} for shortwave forcing over land) of these contrails.

However, detailed in situ optical and microphysical measurements are still needed to evaluate satellite products and to develop more appropriate retrieval algorithm. Discriminating contrails from natural cirrus from satellite observations remains extremely challenging. Although the optical and microphysical properties of young contrails (linear contrails) differ from natural cirrus properties, the contrail properties are highly time dependent and persistent contrail cirrus can be embedded in thin cirrus clouds. Recent *in situ* measurements (Voigt et al., 2017) show that the microphysical properties of contrail cirrus can still be distinguished from natural cirrus at contrail cirrus ages up to several hours.

Most of the studies (Jessberger et al., 2013; Lewellen et al., 2012 ; Schumann et al., 2013) separate the contrail analysis between the two wakes. Primary and secondary wake properties depend strongly on atmospheric conditions and aircraft type (emission index, vortex, flight level, ambient humidity, temperature, …). In the primary wake, contrail ice crystals are quasi-spherical with values of the effective diameter (Deff) typically lower than 4 µm (Schumann et al., 2011; Gayet et al., 2012; Järvinen et al., 2016; Schumann et al., 2017b). The total number concentration of ice particles is typically larger than 1000 cm^{-3} a few seconds after contrail formation (Baumgardner and Gandrud, 1998; Petzold et al., 1997). Then, it decreases by dilution to concentrations below 200 cm^{-3} within less than a minute after contrail generation (Poellot et al., 1999; Schröder et al., 2000; Gayet et al., 2012). Gayet et al. (2012) reported mean values of ice water content of 3 mg m^{-3} and maximum extinction coefficients close to 7 km^{-1}. In agreement with these results, the recent overview on contrail studies presented in Schumann et al. (2017b) reports several microphysical properties at different stages, for different atmospheric conditions as well as comparisons with the Contrail Cirrus Prediction (CoCIP) model simulations. Their study also highlights a large variability (which increases with contrail age) of contrail properties.

Several studies reported findings on the secondary wake and its evolution into contrail cirrus. Detrained from the primary wake and submitted to saturated ambient air with respect to ice, ice crystals grow rapidly, while crystal concentration decreases. Within the first minutes after formation, measurements exhibit aspherical ice crystals characterized by effective sizes up to 6 µm, IWC ranging between 2.5 and 10 mg m^{-3}, extinction between 2 and 3 km^{-1}, with crystal concentrations typically lower than 100 cm^{-3} (Goodman et al., 1998; Voigt et al., 2010; Kübbeler et al., 2011; Gayet et al., 2012; Jeßberger et al., 2013; Schumann et al., 2013; Poellot et al., 1999; Febvre et al., 2009; Kaufmann et al., 2014). Aged contrails can persist and evolve into contrail cirrus if the ambient air is saturated with respect to ice, however those studies are limited by the lack of unambiguous identification (Schumann et al., 2017a).

After a few minutes, tracking contrails by visual navigation is challenging as contrail and contrail cirrus spread in the free troposphere. Observations of the ice crystal shape and growth over several tens of minutes and up to an hour illustrate that crystal effective size can easily reach 20 µm and beyond with number concentrations ranging from 1 to 5 cm^{-3} (Lawson et al., 1998; Schäuble et al., 2009), extinction less than 0.5 km^{-1} (Febvre et al., 2009), and IWC up to 10 mg m^{-3} (Schröder et al., 2000; De Leon et al., 2012). At this stage, within a sustained ice-supersaturated environment, contrail microphysical properties may still differ from those of natural cirrus (Voigt et al., 2017) with concentrations of ice crystals larger than 100 µm in the order of 0.1 cm^{-3}. These crystals typically show bullet rosette type habits (Heymsfield et al., 1998; Heymsfield et al., 2010). Optical depth values can reach values of 2.3 (Atlas and Wang, 2010), corresponding to an extinction of 0.023 km^{-1}. Nevertheless, the transition from contrails to cirrus highly depends on the ambient saturation conditions. Modelling studies with typical atmospheric conditions show a temporal evolution of the optical and microphysical properties when contrails evolve to contrail cirrus clouds (Burkhardt and Kärcher, 2011; Unterstrasser et al., 2016 ; Schumann et al., 2015).

In this study, we report on a powerful alternative to classify cloud events into young contrail, contrail-cirrus and natural cirrus. The method is applied to aircraft data of the CONCERT (Contrail and Cirrus Experiment) campaigns (Voigt et al., 2010, 2011, 2014). The methodology consists in implementing a Principal Component Analysis (PCA) of the angular light scattering data measured by the Polar Nephelometer. The PCA patterns are classified to yield different cluster representing specific contrail types. Corresponding optical, microphysical, and chemical properties are derived for each contrail phase (from young contrails to cirrus contrails). This paper starts with an overview of the properties of contrails and cirrus clouds observed during two specific CONCERT flights (19 November 2008 and 16 September 2011) encompassing a series of different contrail evolution stages. These two flights containing a variety of contrail-cirrus information can be regarded as an analytical framework producing results which then can be compared to contrail-cirrus properties of other flights.

2 CONCERT projects and data processing

2.1 CONCERT campaigns

CONCERT-1 and CONCERT-2 campaigns took place in October/November 2008 and August/September 2011, respectively. These two campaigns with the DLR Falcon 20 E research aircraft were based in Oberpfaffenhofen, Germany, and sampled contrails and cirrus at mid-latitudes over Europe. The overall objective was to reduce uncertainties on the microphysical, chemical, and radiative properties of contrails behind aircraft of different types and to improve the evaluation of contrail's impact on climate. A few CONCERT flights were also dedicated to study emissions of Etna and Stromboli volcanos (Voigt et al., 2014; Shcherbakov et al., 2016). A few stratospheric intrusions were also observed during the flight missions. In total, 23 flights were recorded during the two measurement campaigns, wherein 12 flights were entirely focused on aircraft contrail chasing. Overall, more than 17 different aircraft exhausts plumes have been probed. CONCERT-2 campaign mainly focused on the observation of persistent contrails, and hence on the evolution of contrails to contrail cirrus.

During both CONCERT campaigns, the DLR research aircraft Falcon was equipped with a set of instruments to measure the optical and microphysical properties of cloud particles and also the trace gas composition in the UTLS (Upper Troposphere / Lower Stratosphere) region. Voigt et al. (2010) provide a detailed description of the aircraft instrumentation. We briefly introduce the instruments used in this study.

2.2 Aircraft instrumentation

The microphysical and optical particle properties of contrails and cirrus presented in this study were mainly derived from the PMS Forward Scattering Spectrometer Probe 300 (FSSP-300), the Polar Nephelometer (PN), and the PMS 2D-C hydrometeor imaging probe. The combination of these independent techniques characterizes cloud particles within a range of diameters varying from 0.5 µm to 2 mm.

The PN (Gayet et al., 1997) measures the angular scattering coefficients (non-normalized scattering phase function) of an ensemble of water droplets or ice crystals or a mixture of those particles ranging from a few micrometers to approximately 1 mm in diameter. These particles intersect a collimated laser beam, at a wavelength of 804 nm, near the focal point of a parabolic mirror. The light scattered at angles from 3.49° to 172.5° is reflected onto a circular array of 56 near-uniformly positioned photodiodes. In this study, reliable measurements were performed at 30 scattering angles ranging from ±15° to ±162°. Particle phase (water droplets and/or ice crystals) can be assessed as well as single scattering properties such as the extinction coefficient and the asymmetry coefficient with uncertainties of 25% and 4%, respectively (Gayet et al., 2002; Jourdan et al., 2010).

Particle size distributions and corresponding microphysical and optical integrated properties (IWC, Deff, N, and extinction) were derived from both FSSP-300 and 2DC measurements. The FSSP-300 (Baumgardner et al., 1992) measures the intensity of forward scattered light from cloud particles passing through the laser beam, with cloud particles in the diameter range 0.35-20 µm. In the forward angular region (from 4° to 12°), scattering is mainly described by the particle diffraction pattern and therefore depends on the refractive index, the shape, and the size of the particles. The method of data processing and size calibration used during the CONCERT campaigns have been presented in Gayet et al. (2012). We briefly recall that the asymmetry parameter derived from the PN was used to discriminate nearly spherical particles ($g \geq 0.85$) from non-spherical ones ($g < 0.85$) at 804 nm. For spherical ice particles, Mie calculations were used to derive the size bin limits and the corresponding extinction efficiency. Results were adjusted to the calibrated probe response. Additionally, to minimize Mie ambiguities related to the FSSP-300 size response, 31 channels were rebinned to 13 channels with a diameter ranging from 0.5 µm to 18 µm (upper channels 30 and 31 were excluded from the data analysis). For non-spherical particles, the size of the contrail particles is expressed in terms of an equivalent surface or area diameter, i.e. the diameter of a sphere that has the same area than the projected area of the measured non- spherical particle image (Mishchencko et al., 1997; Schumann et al., 2011). The particles were assumed to be rotationally symmetric ice ellipsoids with an aspect ratio of 0.5. Accordingly, and contrary to the method used for spherical particles, 15 size bins ranging from 0.5 µm to 18 µm were defined based on T-Matrix calculations following Borrmann et al., (2000).

The bi-dimensional optical array spectrometer probe (2DC) provides information on the crystal size and shape within a nominal size range from 25 µm to 800 µm by recording cloud particles shadow images with a 25 µm resolution. The method of data processing used in this study is described in detail in Gayet et al. (2002) and Febvre et al. (2009). Reconstruction of truncated particles has been considered for the PSD calculations and the sampling surfaces have been derived according to Heymsfield and Parrish (1978). To improve the statistical significance of low particle concentrations, a 5-s running mean was applied. As the sensitivity of the probe to small particles decreases with airspeed (Lawson et al., 2006), particles smaller than 100 µm may not be detectable at the Falcon airspeed of typically 180 m s^{-1}. This may result in larger uncertainties of up to 100% in the derived microphysical parameters such as the IWC (Gayet et al., 2002 and 2004).

For spherical and non-spherical particles, the extinction coefficients are calculated from the following equation:

$$Ext = \frac{\pi}{4}\sum_i \beta^i_{ext} N_i D_i^2 \quad (1)$$

where β^i_{ext} is the extinction efficiency (values depend on spherical or aspherical particle characterization), D_i the mean diameter in channel i, and N_i the number concentration.

Different approaches are used to retrieve ice water content from spherical and non-spherical particles (Garret et al., 2003 ; Gayet et al., 2004 ; Gayet et al., 2012). For spherical particles (gPN > 0.85), IWC is computed from the following equation:

$$IWC_{spherical} = \frac{\pi}{6}\rho_{ice}\sum_i N_i D_i^3 \quad (2)$$

with ρ_{ice} the bulk ice density (0.917 g cm^{-3}).

For non-spherical ice crystals (gPN < 0.85 and for particle diameters larger than 70 µm), an equivalent diameter method is used (Gayet et al., 2004). For an ice crystal with an area A, the particle equivalent diameter D_{equ} (in mm for eq. (3) and (4)), the equivalent mass x_{equ} (in mg), and the Ice Water Content (IWC in mg m^{-3}) are defined as:

$$A \leq 0.049\ mm^2 \qquad D_{equ} = 0.82A^{0.48} \quad (3)$$

$$A > 0.049\ mm^2 \qquad D_{equ} = 0.56A^{0.32} \quad (4)$$

$$x_{equ} = \frac{\pi}{6}\rho_{water} {D_{equ}}^3 \quad (5)$$

$$IWC_{non-spherical} = \sum_i N_i x_{equ} \quad (6)$$

with ρ_{water} the bulk water density (1 g cm^{-3}).

These equations do not account for possible shattering of large ice crystals on the probe inlets. This effect is minimized in young contrails but can lead to an overestimation of small ice crystal concentration in contrail cirrus clouds.

Trace gas measurements were also performed. NO/NO_y concentrations can be significant in young tropospheric aircraft plumes. NO and NO_y mixing ratio were performed using the chemiluminescence technique (Schlager et al., 1997) with a time resolution of 1 s. Instruments used for CONCERT campaigns are described in several studies (Jurkat et al., 2010 ; Jurkat et al., 2011 ; Voigt et al., 2014 ; Jurkat et al., 2016). The accuracy (and precision) of the NO and NO_y measurements are estimated with 7% (and 10%) and 10% (and 15%), respectively (Ziereis et al., 2000).

Relative humidity with respect to ice (RHI) is also key parameter to understand contrail formation and microphysical properties. Water vapour was measured with the chemical ionization mass spectrometer AIMS-H2O during CONCERT-2 (Kaufmann et al., 2014; 2016). Hygrometers using the Lyman-α technique (FISH, Zöger et al., 1999; Meyer et al., 2015), and frost point hygrometers (CR-2, Heller et al., 2017) were deployed on the Falcon during CONCERT-1 and 2.

3 **Results**

3.1 **Overview of the cloud properties sampled during the reference cases**

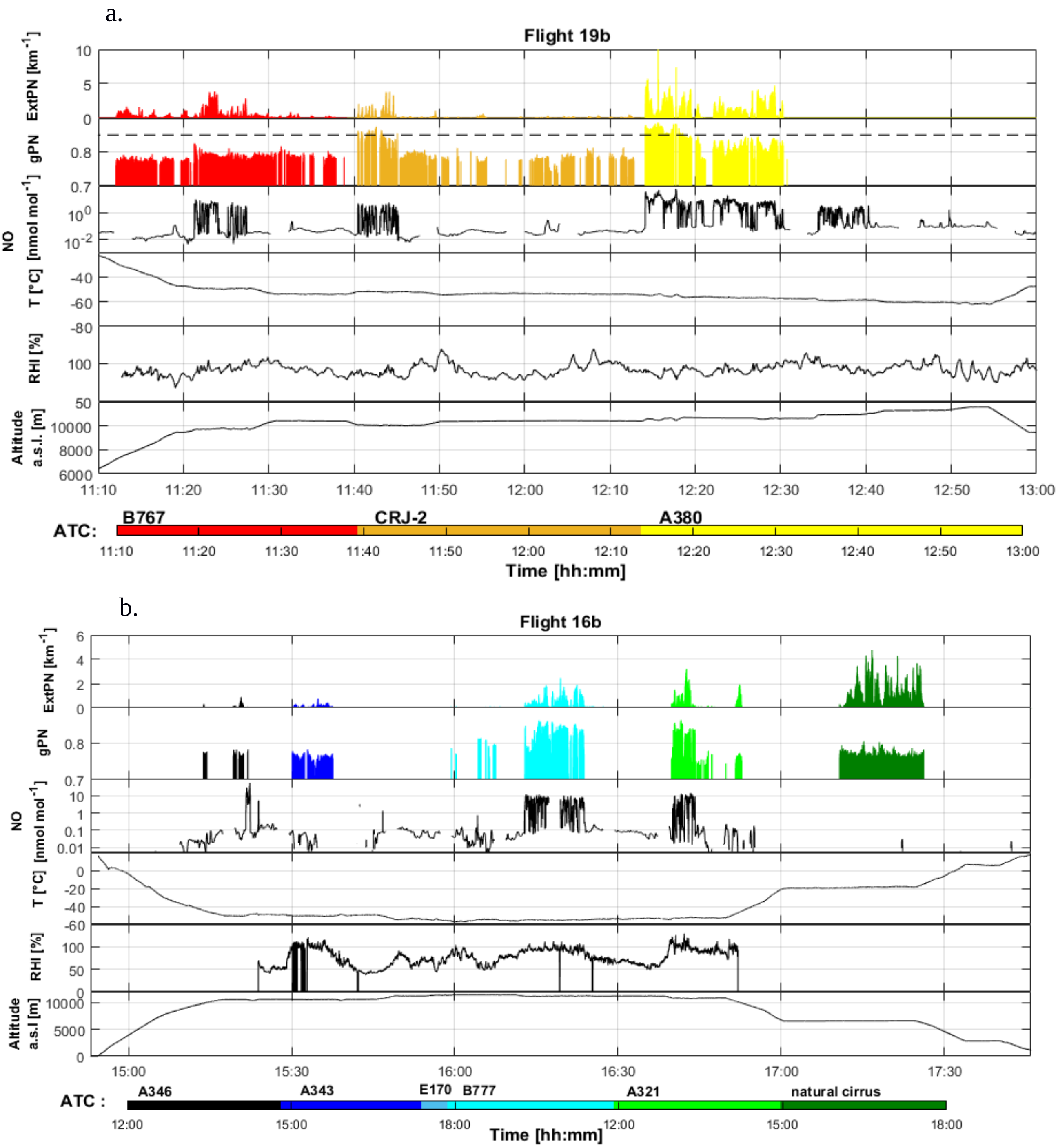

Figure 1: Time series at 1 s resolution for flights a) 19b (CONCERT 1) and b) 16b (CONCERT 2). From top to bottom: extinction coefficient (in km^{-1}) and asymmetry parameter measured by the Polar nephelometer at 804 nm (dashed line corresponds to a 0.85 value), concentration of nitric oxide (in $nmol\ mol^{-1}$) measured by chemiluminescence technique, temperature (in °C), relative humidity with respect to ice (in %), and altitude a.s.l. (in m). Temporal series are coloured according to time and aircraft chasing information from Air Traffic Control (ATC).

The purpose of this section is to give an overview of the contrail optical properties and more interestingly to evaluate the ability of the Polar Nephelometer measurements to identify contrails. Two flights, performed on 16 September 2011 during CONCERT-2 (flight 16b) and on 19 November 2008 during CONCERT-1 (flight 19b), respectively, were selected for their variety of contrails and cirrus sampled during these two flights. The two flights are considered as a benchmark to illustrate the potential of the PCA methodology described in Sect. 3.2.

Figure 1 displays the time series of the extinction coefficient (ExtPN) and the asymmetry parameter (gPN) at a wavelength of 804 nm, relative humidity with respect to ice (RHI), the nitric oxide (NO) concentration, the temperature T and the altitude for flights 19b and 16b. RHI measured with the AIMS mass spectrometer is shown for flight 16b. RHI measurements during flight 19b as well as instrument shortcomings are discussed in details in Kübbeler et al. (2011), Gayet et al. (2012), Jessberger et al. (2013) and Schumann et al. (2013). For both flights, Air Traffic Control (ATC) provides information on the flight tracks and on the chased aircraft (aircraft type, engine type, fuel flow, weight, engine power setting). Form this information the Falcon measurements were attributed to the exhaust plume of individual aircraft with an estimated plume age. Time series are colour coded according to ATC information.

The PN extinction coefficient coupled with the asymmetry parameter seems to be a reasonable proxy to detect contrails and cirrus clouds (see amongst other references, Voigt et al., 2010). ExtPN values, by definition, depend on the cloud particle concentration and size. Values typically beyond 0.1 km^{-1} correspond to cloud events that are well correlated to environmental conditions supersaturated with respect to ice (RHI > 100%). Figure 1 shows that relatively high values of extinction can be found in flights 19b and 16b that are linked to the presence of contrails or cirrus clouds. Moreover, the temporal distributions of these values are in accordance with ATC information for both flights. For instance, most of the contrails induced by commercial aircraft exhaust plumes are associated with significant extinction coefficient values. The ExtPN values are between 0.2 km^{-1} and 10 km^{-1} for contrails induced by A346, A340, and A380 commercial aircraft. Cirrus clouds are detected with more variable extinction values mostly larger than 0.5 km^{-1}. Most of the aircraft induced contrails are detected by the PN except for the ones stemming from the E170 airplane. At 15:50 during flight 16b, ATC identified the E170 position close to the Falcon flight trajectory, however the ExtPN and the NO mixing ratio remained very low. Hence, the E170 contrail was not probed by the Falcon. In the following we assume that only periods with ExtPN values above 0.1 km^{-1} are considered as a reliable signature of contrails.

The absolute values of the asymmetry parameter gPN provide additional information on the cloud particle shape. Indeed, gPN is a good indicator of the degree of sphericity of ice crystals (Gayet et al., 2012). Ice clouds with gPN values higher or equal to 0.85 are typically composed of spherical ice crystals, whereas lower values are indicative of aspherical ice particles. In a supersaturated environment, crystals grow by water vapour deposition and become increasingly aspherical with time. However, in very young contrails, spherical ice crystals with an asymmetry coefficient around 0.85 prevail. gPN is decreasing when water vapour diffusion is generating more and more aspherical crystal shapes at ice supersaturation. This can be observed for A321 chasing during flight 16b where gPN is decreasing to a value of 0.75 whilst RHI remains around 100%. This is not the case during B777 chasing where no gPN decrease is observed when RHI < 100%. However, it is important to note that the RHI measurements during the CRJ-2 chasing events do not show supersaturated conditions, whereas contrail seems persistent. Indeed, RHI measurements should be discussed carefully for this campaign due to calibration issues.

Natural cirrus clouds are mainly composed of non-spherical ice crystals. These clouds can be easily discriminated from young contrails as they exhibit a much lower asymmetry parameter typically below 0.75 (see amongst others Jourdan et al., 2003b, Febvre et al., 2009). However, no accurate ambient RHI data can be retrieved for measurements in natural cirrus due to instrumental calibration problems. A good example of the evolution of gPN is the CRJ-2 contrail observed between 11:40 and 11:45 during flight 19b. The sequence illustrates the potential of the gPN measurement to characterize the evolution of contrail properties. The evolution of the ice crystal shape is reflected in the decrease of the asymmetry parameter from 0.88 to 0.79 (uncertainties around 0.04) after only 5 min and down to 0.77 after 20 min. A weaker decrease of gPN values (around 0.78 ± 0.02) is then observed until 12:10 corresponding to 30 min of contrail ageing. During this period, ice crystals are expected to grow by water vapour diffusion. A similar decrease of gPN values has been reported by Gayet et al. (2012) in the ageing contrail from an A380 aircraft, and is also visible in the present study for the B767 and the A321 contrails.

NO concentration measurements can also be used to discriminate natural cirrus clouds from ice clouds influenced by aircraft traffic. At the typical altitude of 10 km, NO environmental concentrations are close to background values. In contrast, NO concentrations in young contrails may reach several tens of nmol mol^{-1} (Voigt et al., 2010). Figure 1 shows a good correlation between the expected localization of young contrails and NO concentrations. The dilution effect in the upper troposphere causes an important decay of chemical concentrations. For instance, the first few seconds of the A380 chasing during flight 19b are characterized by a high NO concentration (up to 40 nmol mol^{-1}) followed by a fast decrease to 10 nmol mol^{-1} in the next 15 min, and less than 5 nmol mol^{-1} beyond 15 min. NO concentrations finally decrease to background levels within hours (e.g. Voigt et al., 2017). This decrease of the NO concentration is in accordance with the decrease of the extinction coefficient (from 10 to 0.2 km^{-1}) and asymmetry parameter (from 0.88 to 0.77). NO is mainly used as an additional contrail indicator. However, during some aircraft chasing events, NO concentrations were near background levels, while mass spectrometric measurements (not shown here) indicate elevated concentrations of HONO, HNO_3, and SO_2 representative for contrail chemical species.

Flights 19b and 16b clearly show that the optical properties of contrail clouds (supported by the ATC information) in conjunction with specific trace gas concentration measurements can be used to discriminate contrails from natural ice cloud events. A first order analysis of these parameters can be used to roughly distinguish young contrails (mostly quasi-spherical ice crystals) from aged contrails (mostly aspherical ice crystals) and natural cirrus (background NO concentrations). This analysis is mainly qualitative and based solely on a few typical parameters (Fig. 1). A more robust statistical method should be used to accurately separate the different contrail phases from natural cirrus. In the following section, relationships between contrail and ice cloud properties scattering properties are investigated more extensively to assess whether the information content of the PN scattering measurements is sufficient to document changes in the contrail microphysical properties.

3.2 Statistical Method

In this section, we present a methodology based on the statistical analysis of the optical signature of contrails and cirrus. The goal is to classify the contrail properties according to the aircraft origin and evolution stage. The main objective of the Principal Component Analysis (PCA) is data reduction to allow a better physical interpretation of the light scattering patterns derived from the Polar Nephelometer measurements (Legendre and Legendre, 1998; Jourdan et al., 2003). In this study, optical properties of ice crystals in the evolving contrail environment are examined to evaluate contrail evolution. This statistical analysis was already successfully applied to discriminate mixed phase clouds (Jourdan et al., 2003 ; Jourdan et al., 2010) from liquid clouds and ice clouds, and to identify porous aerosol in degassing plumes (Shcherbakov et al., 2016).

3.2.1 Reference definition

The PCA is first applied to the PN angular scattering coefficients measurements performed during flights 16b and 19b which are here considered as our reference dataset. Initially, a correlation matrix is calculated to characterize the link between each scattering angle. The PCA is designed to generate a new limited set of uncorrelated parameters, called principal components C_{lj} representative of the original data set variability.

A first implementation of the PCA is performed to detect unreliable data or out of order photodiodes. For instance, seven photodiodes presented a low signal to noise ratio and were excluded from the dataset. Flight sequences characterized by ExtPN<0.1 were also removed. Finally, flight sequences dedicated to aircraft chasing and ice cloud sampling were considered to perform a second PCA. The analysis is performed on the remaining angular scattering coefficients (4669 Angular Scattering Coefficients (ASC) representing PN measurements of flights 16b and 19b) restricted to 25 angles θ ranging from 15° to 155°. The new set of variables or coordinates, C_{lj}, can be expressed with the scalar product of the vector of reduced angular scattering coefficients$\overrightarrow{\sigma_j}(\theta)$ for the j^{th} measurements, expressed in log scale, and the l^{th} eigenvector $\xi_l(\theta)$ (i.e. principal component) of the total data set correlation matrix (Jourdan et al., 2010).

$$C_{lj} = (\overrightarrow{ln\sigma_j} - \langle\overrightarrow{ln\sigma}\rangle)^T . \overrightarrow{\xi_l} \quad (4)$$

where $\langle\overrightarrow{ln\sigma}\rangle$ represents the average ASC of the dataset.

The first three eigenvectors $\overrightarrow{\xi_l(\theta)}$of the correlation matrix are displayed in Fig. 2 along with their normalized eigenvalues λ_l, representing more than 99% of the variability of the PN angular scattering coefficients (ASC).

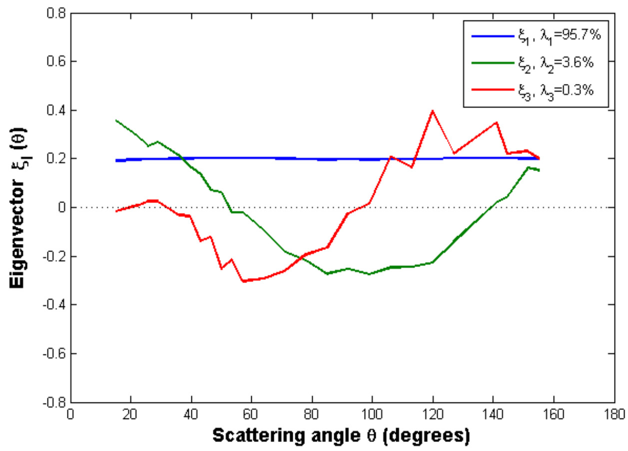

Figure 2: First three eigenvectors for the flights 16b and 19b.

The first eigenvector $\xi_1(\theta)$ is approximately constant versus scattering angle and represents 95.7% of the total variance. It means that this principal component is representative of changes of the magnitude of phase functions without any changes in their global shape. This behaviour means that 95.7% of the ASC variations are linked to changes of the cloud particle extinction. Results show a good correlation ($r^2 = 0.98$) between the first eigenvector and the extinction derived from the PN measurements (ExtPN).

The second eigenvector $\xi_2(\theta)$reverses sign twice at scattering angles equal to 50° and 140° with an extremum around 90°. Accordingly, 3.6% of the angular scattering variability corresponds to a redistribution of scattered energy from the angular region (50°-140°) to scattering angles lower than 50° and higher than 140°. Light-scattering modelling studies demonstrate that the scattering behaviour in the angular region between 60° and 140° is sensitive to the particle shape and thermodynamic phase (Jourdan et al., 2010). A strong linear correlation (r^2=0.97) between the second eigenvector and the asymmetry coefficient (gPN) at 804 nm is found.

The third eigenvector represents only 0.3% of the total variance. However, this eigenvector provides additional information in scattering regions which are not well described by the first two principal components. It has opposite signs in the angular region (30°-90°) and (90°-155°) with maximum extremal values at 60° and 120°. The shape of the third eigenvector describes the forward/backward hemisphere partitioning of the scattering. Baran et al. (2012), Xie et al. (2006), and Xie et al. (2009) showed that the scatter pattern for angles between 120° and 160°, corresponding to ice bow-like effects, is sensitive to quasi-spherical particles. Moreover, these backscattering angles (θ>120°) and scattering angles around 22° and 46° (corresponding to halo features) can also be linked to the particle habits and surface roughness (Xie et al., 2009, Jourdan et al., 2010).

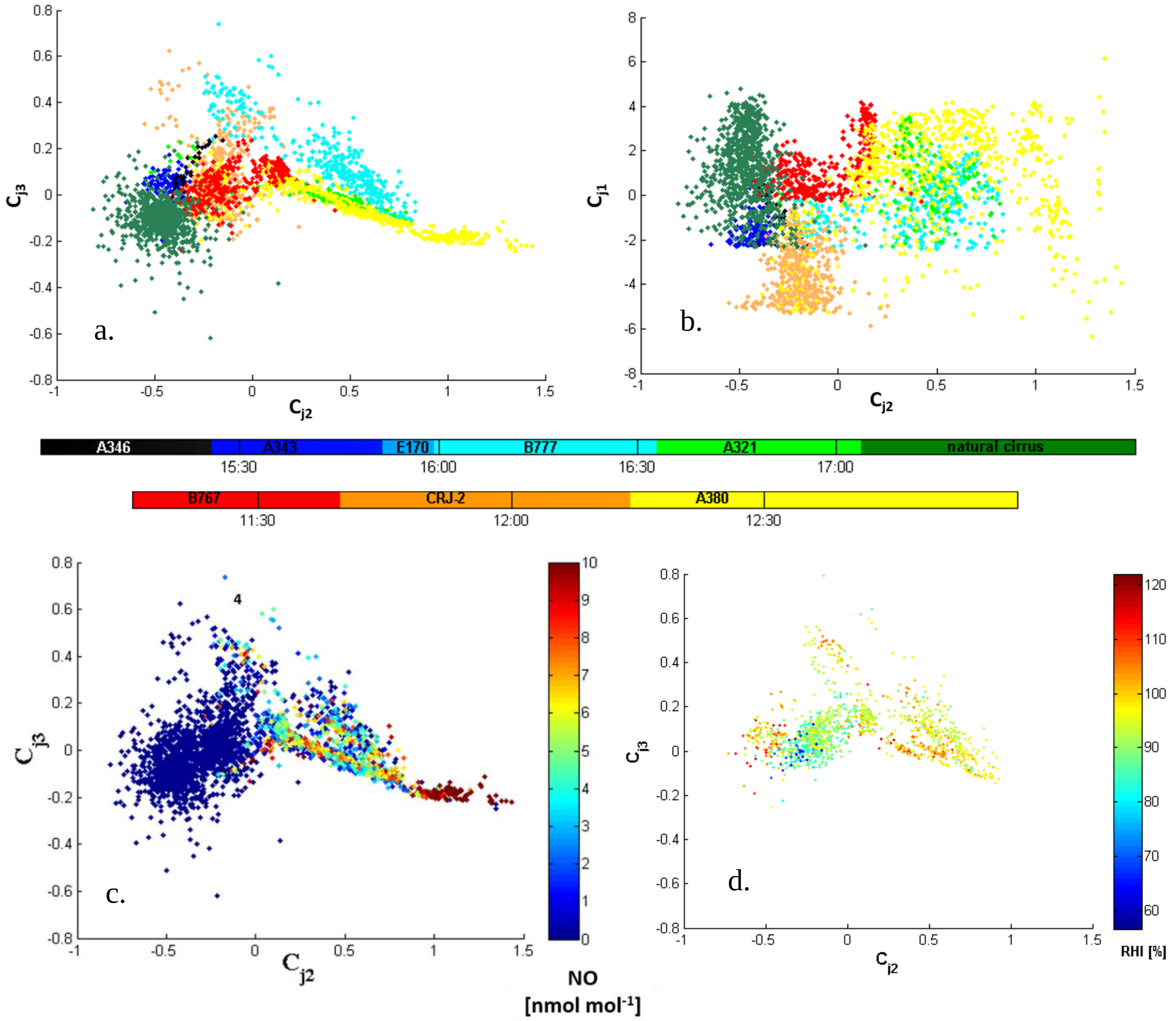

Figure 3: Expansion coefficient diagram for flights 16b and 19b: third versus second principal component for a), c) and d), and first versus second principal component for b). Data points are colour coded according to ATC information for a) and b), by NO concentration for c), and by RHI values for d).

Each phase function (or ASC) measured by the PN can be expressed with a good accuracy as a linear combination of the three principal components (Jourdan et al., 2010). The PN data are projected into a new space defined by the three principal components (3D-space) instead of the 25-dimensional space of ASC. The scatterplots of the C_{j3} and C_{j1} expansion coefficients versus the C_{j2}

coefficient are represented on Fig. 3a and b respectively. Fig. 3a illustrates the features of the ASC measurements in one of the most comprehensive way. Each point corresponds to a measured phase function documented over 25 angles. The variability of C_{j2} coefficients is significant with values ranging from -1 to 1.5. The angular variation of the second principal component indicates that large values of C_{j2} ($C_{j2} > 0.75$) correspond to ASC with low side scattering (60°-130°) and higher forward scattering (15°-40°) and somehow higher backscattering (145-155°). This behaviour is connected to an increase of the asymmetry parameter with an increase of C_{j2} values. Thus, the fraction of spherical particles increases with increasing C_{j2}. In the region defined by negative values of C_{j2} the density of points is relatively high. These cloud events exhibit optical properties characterized by a large side scattering and low asymmetry parameter. Therefore, specific cloud sequences sharing similar scattering properties can be identified based on this second principal component. Young contrails characterized by quasi-spherical ice crystals have high positive values of C_{j2} while cirrus clouds and contrail cirrus exhibit high negative values.

In the space of the third principal component high positive values of C_{j3} imply that less energy is scattering in the forward hemisphere and thus more energy is scattered in the backward hemisphere. The variability of the expansion coefficients is less pronounced as ASC are distributed between -0.4 and 0.6. Most of the measured ASC do not significantly differ from the average ASC in the angular ranges (30°-90°) and (90°-155°). However, some specific clusters linked to scattering behaviour can be identified for values of C_{j3} greater than 0.1 and lower than -0.1. These threshold values also depend of the position of the ASC on the second principal component. Finally, the first principal component is directly linked to the extinction coefficient. High values of C_{j1} are representative of optically dense cloud sequences.

Figure 3c shows an increase of C_{j2} for increasing NO mixing ratio. This clearly indicates that the contrails are evolving in space and/or time along the Falcon flight track. Cloud regions influenced by air traffic can be discriminated from clouds formed by natural processes based on the NO concentration values. Hence, contrails characterized by a low side scattering due to the presence of spherical ice crystals correspond to high NO concentration. This behaviour can be a signature of young contrail properties. Elder or aged contrails composed of a higher fraction of non-spherical crystals or growing more aspherically are expected to exhibit an enhanced side scattering and a lower asymmetry parameter associated to lower NO concentrations. RHI measurements also give relevant information on the capacity of the cloud to be persistent. Thus, Fig. 3d shows higher RHI values with decreasing gPN values.

3.2.2 Clustering analyses

The new representation of each measurement in the space of the first three principal component reveals different clusters, characteristic of specific scattering behaviour. The clustering k-mean method (Seber 1984, Spath 1985) is applied to the reference dataset (fights 19b and 16b) to partition the observations into k clusters to minimize the variance within each cluster (i.e. to minimize the distance between each data point and the centre of the cluster it belongs to). The number of cluster k is an adjustable parameter. Then in a first step, each observation is assigned to a specific cluster whose mean has the least squared Euclidean distance (i.e. nearest mean). In a second step, the position of each cluster is set to the mean of all data points belonging to that cluster (i.e. the centroids of each of the k clusters becomes the new means). These two steps are repeated until convergence is reached when the assignments no longer change.

16 clusters were found to encompass all points of the two flights and to partition each aircraft chasings identified from ATC information (Fig. 3a and 3b). For clarity and better understanding of the variability of contrail properties, we choose to limit the number of clusters to

6. 9 clusters are merged into 2 clusters to define the group "natural-cirrus" and B767 / A343 / CRJ-2 contrails (referred hereafter to Cluster 3 and 5 respectively). 4 clusters are also gathered in one new cluster corresponding to A321 / A380 contrails (referred to Cluster 2 hereafter). In addition, only data within the 10% of the maximum Mahalanobis distance (De Maesschalck et al., 2000) to the respective cluster's centre has been considered for this analysis.

Clusters are defined by their means (or centres), standard deviations (or widths), and cross-correlations (or tilts). The Mahalanobis distance is given by the equation:

$$D_M(x)_i = \sqrt{(x - \mu_i)^T S_i^{-1} (x - \mu_i)} \qquad (5)$$

with D_M the Mahalanobis distance between point χ and the i[th] cluster center, μ_i the N-dimensional mean of this cluster and S_i its covariance matrix.

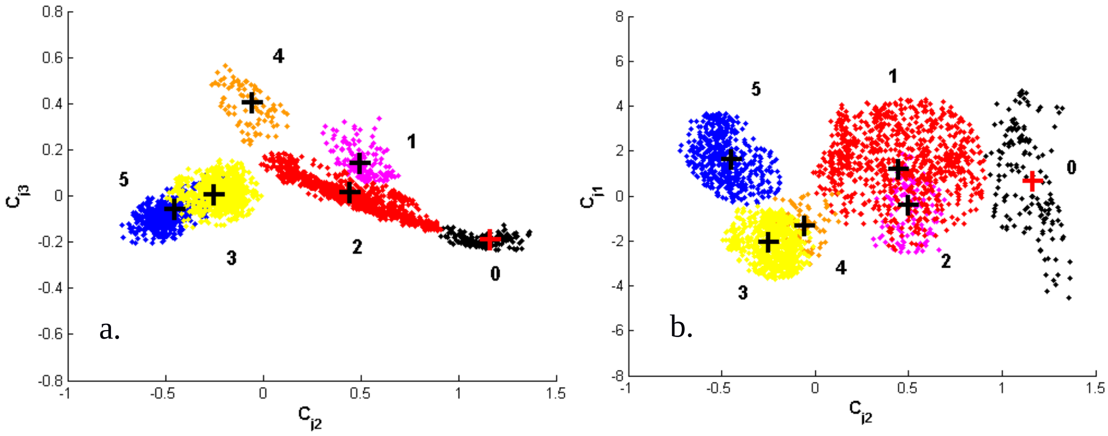

Figure 4: Clustering results of the k-mean method applied to the base (flights 16b and 19b). Third versus second principal component for a), and first versus second principal component for b). Only data within the 10% of the maximum Mahalanobis distance to the respective cluster's centers have been considered for this analyse.

Figure 4 shows the partitioning of the dataset into the 6 new clusters (clusters 0 to 5). In the following we use data from chemical tracers and optical measurements, and aircraft type information to support and discuss the results of the k-means clustering method.

While clusters 3 and 5 are characterized by very low NO concentrations (close to zero, Fig. 3c) above background, clusters 0, 1, 2, and 4 correspond to higher concentrations representative of a significant aircraft exhaust influence. ATC information shows that cirrus clouds are gathered in cluster 5. Most of the contrails induced by the B767, A343, A346 and CRJ2 aircraft are associated to cluster 3 or 5. These cloud events share similar optical properties characterized by a low asymmetry parameter, high side scattering behaviour, and supersaturated ambient conditions with respect to ice for some cases. Contrails relative to the A380 aircraft are dispatched in cluster 0 and 2 while the ones corresponding to the B777 are spread out between clusters 1 and 4.

The contrail and cirrus classification based on ASC measurements appears to be consistent with the independent trace gas measurements. Each cluster represented on Fig. 4 can be linked to a distinct cloud event. Therefore, the combination of flights 16b and 19b can provide a relevant test-bed database to discriminate contrail properties. Young contrails (spherical ice crystals) are associated to clusters 0, 1 or 2, whereas aged contrails (aspherical ice crystals and high RHI values) with more pristine ice are categorized in clusters 3 and 4, and finally natural cirrus (low NO concentrations) are found in cluster 5. A less precise analysis (using onboard camera) reveals that cluster 0 corresponds essentially to the primary wake created below the secondary wake behind an aircraft. Table 1 summarizes these cluster's definitions and names used in this work.

Cluster number	definition	name
0	Primary Wake	**PW**
1	Young Contrail 1	**YC1**
2	Young Contrail 2	**YC2**
3	Aged Contrail 1	**AC1**
4	Aged Contrail 2	**AC2**
5	Cirrus Cloud	**CC**

Table 1: Cluster's definitions according to ATC information and tracer measurements (NO concentrations and RHI values)

One should keep in mind that some points are still arbitrarily attributed to a particular cluster without strong physical justification.

3.2.3 Merging other CONCERT flights

In this section we complement the previous analysis with additional cloud optical measurements performed during other CONCERT flights to increase the robustness of the method.

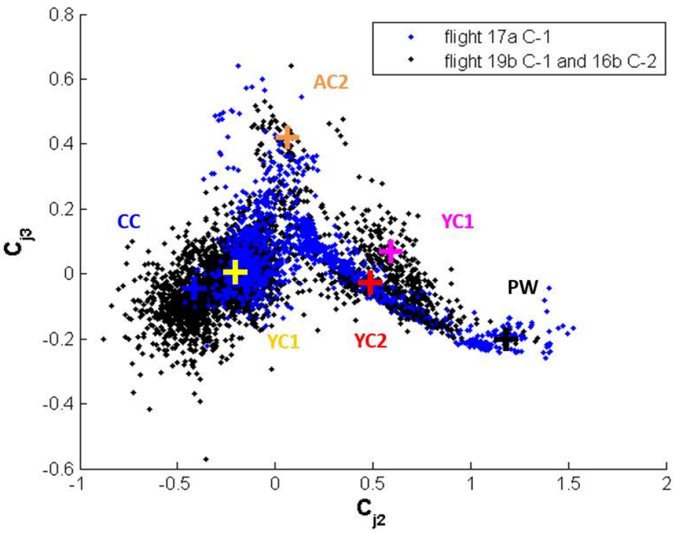

Figure 5: Example of data projection in the C_{j2}/C_{j3} space where data from flight 17a (blue data points) are superposed on the data from the benchmark flights 19b and 16b (black data points).

The ASC measured during other flights can be projected in the space of the principal components established with flights 16b and 19b dataset. The coordinates of the data points corresponding to the other flights are calculated from Eq. (4). An example of this data projection is illustrated in Fig. 5 where flight 17a is represented in the C_{j2}/C_{j3} space. Each data point can be attributed to one cluster previously defined by the k-mean clustering method based on flights 16b and 19b dataset (black points). In other words, the ASC measured during another flight can be merged (projected) into the expansion coefficient diagram displayed on Fig. 3. Data points sharing similar optical properties will be close to each other on such plot. Figure 5 shows that different contrail phases are observed during flight 17a. Data points are mostly grouped into cluster AC1, but are also present in clusters AC2, YC2, and PW. Finally, cloud data gathered during this flight are mainly categorized as young and aged contrails. We follow this methodology to project and classify each additional "contrail" event performed during both CONCERT campaigns with minimum Mahalanobis distance (see Eq. (5)).

Day / Aitcraft		Cluster: PW (1st wake)	YC1 (young contrails)	YC2 (young contrails)	AC1 (aged contrails)	AC2 (aged contrails)	CC (Cirrus)	Number of points	Age (s)
17a C-1	TOTAL							1435	
	A340-311							359	61 - 144
17b C-1	TOTAL							2715	
	B737-500							310	77 - 151
	A340-642							100	82 - 139
	NC							189	-
19a C-1	TOTAL							2152	
	A319-111							628	94 - 129
	A340-311							175	63 - 90
19b C-1	TOTAL							1647	
	B767-300							319	77 - 107
	CRJ-2							151	80 - 95
	A380-841							677	109 - 240
20 C-1	TOTAL							1434	
	B737-300							64	90 - 290
16b C-2	TOTAL							1511	
	A340-600							128	100 - 132
	B777							378	120 - 160
	A321							135	70 - 95
17 C-2	TOTAL							2904	
	NC1							498	-
	NC2							233	-
24 C-2	TOTAL							1380	
	B777							371	112 - 178

Table 2: Classification relative to the six clusters on the Cj2/Cj3 representation of the PCA of all data points for each flight of the two CONCERT campaigns (C-1 in November 2008 and C-2 in September 2011). The legend of the bars represents the relative contribution of data points of individual contrails (blue bars) and also entire flights (black bars) to the 6 individual clusters.

The assignment of the data points to the six clusters shown on the expansion diagrams is summarized in Table 2. 8 flights (6 additional flights) representing 4426 ASC measurements were processed. The lengths of the bars in Table 2 represent the distribution of the data points within the different clusters: a) black bars correspond to the fraction of cloud events within a specific flight (with extinction coefficient higher than 0.1 km^{-1}) and b) blue bars represent cases of individual contrails within the flight. Data points with extinction coefficient lower than 0.1 km^{-1} are not shown in the table. More than 30% of the data points are located in clusters AC1 and/or CC meaning that they correspond to aged contrail and sometimes natural cirrus. Flights clearly performed in well visible contrails outside natural cirrus (earlier development stage and/or intensified persistent elder contrails) exhibit significant fraction of data points associated to clusters PW, YC1, and YC2 (young contrails) for both CONCERT-1 and CONCERT-2 campaigns. However, within these flights data points are also gathered in cluster AC1 (aged contrails clean) and to a lesser extent in cluster AC2 (aged contrails, mostly corresponding to measurements performed during two different B777 contrail chasing events).

These results are in reasonable agreement with previous conclusions (this subsection) drawn for the cluster definitions and associated contrail / ice cloud characteristics. Very young contrails have been mostly chased during CONCERT-1 (flights 19a and 19b). Another interesting result is related to flight 17 during CONCERT-2 (flight 17 C-2) where no aircraft information was provided by ATC. Still ATC data indicate measurements in exhaust plumes and the Falcon flew apparently in visible contrails (ExtPN > 0.1 km^{-1}) which were probably too old for ATC recognition. Our analysis shows that these data points can mainly be attributed to cluster CC and AC1. This observation suggests that significantly aged contrails have been sampled. However, crystal formation and growth processes in contrails and natural cirrus suggest that very old contrails more and more resemble natural cirrus properties.

ATC information on exhaust plume ages was also collected during each chasing. Some chasings were performed less than 100 s after contrail formation. This is the case for the A340 contrail during flight 19a and for the CRJ-2 contrail during flight 19b of CONCERT-1 and for the A321 contrail during flight 16b of CONCERT-2. One can notice that the contrail ages are well correlated to the chosen cluster definitions, revealing that contrail data relative to the A340 are included in cluster PW and YC2 (young contrails) for more than 90% of the data points, and nearly 63% for the CRJ-2 and 84% for the A321. According to our cluster classification, only 5% of the data points gathered during these three flights correspond to aged contrail (cluster AC1 and AC2) categories in contrast to other CONCERT-1 and CONCERT-2 flights (with more than 30% of data points associated to AC1 and AC2). Even though it is still difficult to associate contrail ages to measurement points, the "contrail age" ranges agree with the cluster definitions.

4 Evolution of contrail properties

4.1 Optical and chemical cluster properties

In the previous section we showed that cloud events can be separated according to their light-scattering properties. Six clusters were defined based on two flights having a significant number of data points distributed in each cluster. In this section we present the mean optical, chemical, and microphysical properties for each cluster. The average properties are calculated for all data points associated to the 6 individual clusters (all flights, both CONCERT campaigns). Figures 6a, 6c, and 6d show the normalized frequency distributions of the asymmetry parameter (gPN), the extinction coefficient (ExtPN), and NO concentrations for the six clusters, respectively. Figure 6b represents the mean normalized scattering phase functions of each clusters. However, it should be noted that the number of data points could differ significantly from one cluster to another (from 141 measurements for Cluster YC1 to 8950 measurements for Cluster AC1).

The asymmetry parameter gPN statistics shown in Fig. 6a provide the most striking evidence of the relationship between contrail evolution stage and optical properties. In agreement with findings of Gayet et al. (2012), aged contrails (cluster AC1 and AC2) and natural cirrus (cluster CC) correspond to gPN values ranging from 0.72 to 0.80. Younger contrails (cluster YC1 and YC2) have values of gPN of 0.80 to 0.86. Values of the asymmetry parameter in the primary wake (cluster PW) are typically above 0.86. These features are a consequence of the time evolution of ice crystal shapes from quasi-spherical ice particle after exhaust to non-spherical (e.g. column, needle, bullet, and bullet-rosette type crystals) as the contrail evolves. In the primary wake, the pressure increases in the descending vortex. This leads to adiabatic heating and subsequent sublimation of the ice crystals (Lewellen and Lewellen, 2001; Unterstrasser et al., 2016) that can explain the spherical shapes of ice crystals and thus, the high values of the asymmetry coefficients.

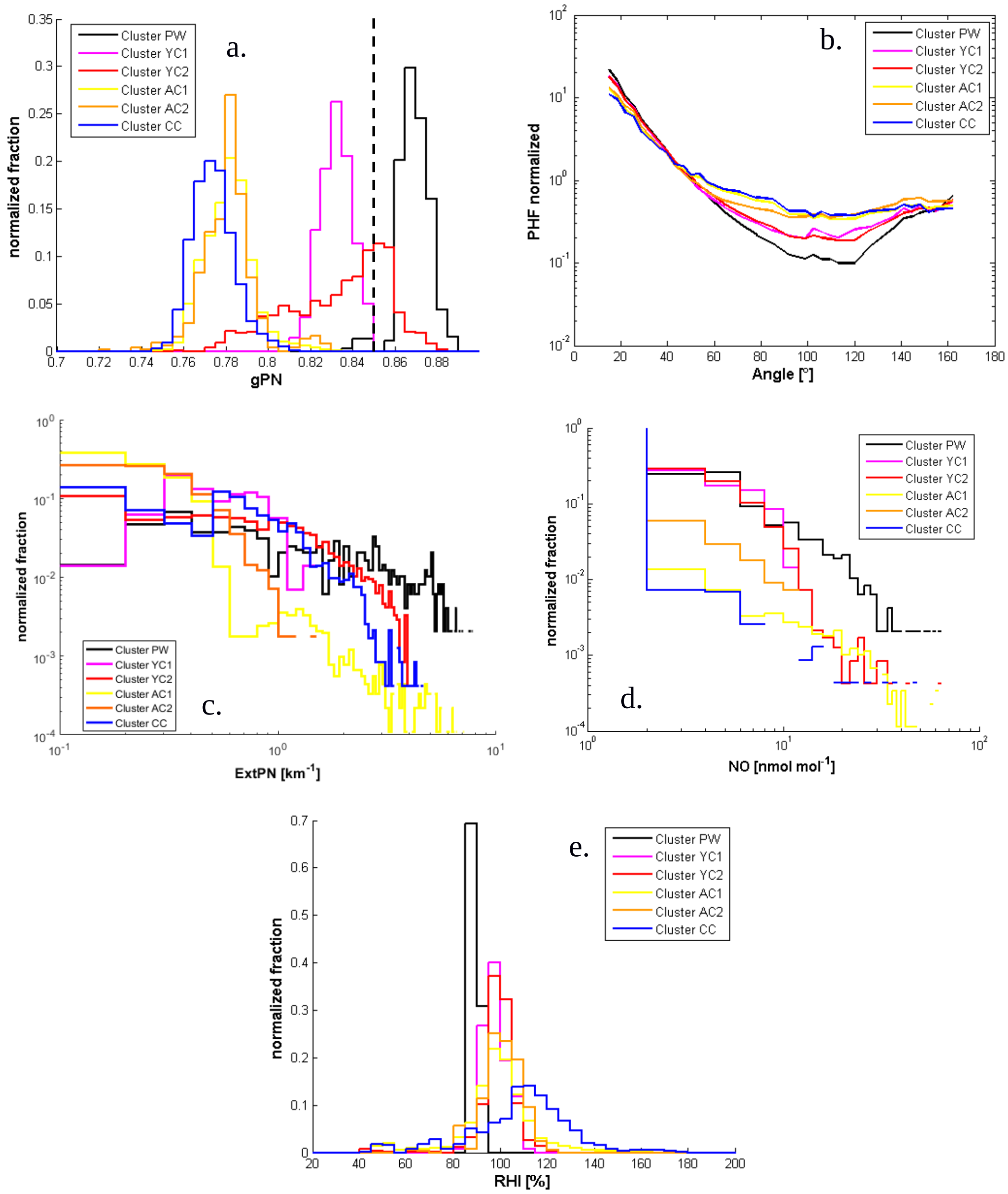

Figure 6: Normalized histograms of a) asymmetry coefficient (dashed line corresponds to a value of 0.85), b) phase function, c) extinction retrieved by Polar Nephelometer, d) NO concentration for all flights, and e) RHI conditions for CONCERT-2 flights.

The normalized phase functions are presented in Fig. 6b. Primary wake phase functions (cluster PW) are clearly different from the young contrail phase functions (cluster YC1 and YC2), which are themselves different from aged contrails (cluster AC1 and AC2) and natural cirrus (cluster CC) phase functions. The main difference is observed in the side scattering region (50°-140°). This region is related to changes of ice particles shapes and to the fraction of spherical ice crystals within the contrails. This behaviour is expected and agrees with the position of clusters PW, YC2 and YC1 on the expansion coefficient diagram (Fig. 2). Indeed, the decrease of the C_{j2} coefficient is associated to a side scattering enhancement. Therefore, very young contrails are composed mainly of spherical ice crystals for which the phase functions indicate a substantial scattering at forward angles and much lower scattering at sideward angles. As the contrails evolve, these features smooth out leading to phase functions with a featureless flat behaviour at side scattering angles. Finally, the averaged normalized phase functions of old contrails and natural cirrus are similar to each other. This also explains that they are difficult to discriminate within the PCA.

The extinction coefficient statistics are presented in Fig. 6c. All the aged contrails (cluster AC1 and AC2) exhibit extinction coefficients lower than 2 km^{-1}. Also 80% of the sampled natural cirrus (cluster CC) show such low extinction coefficients. For younger contrails (cluster YC1 and YC2), the extinction coefficients can reach 5 km^{-1}. Largest extinction coefficients are found in primary wake measurements (cluster PW) with values up to 8 km^{-1}. Still, the main fraction (more than 50% of data points) of young contrail data yields extinction coefficients from 0 to 1 km^{-1}.

Concentrations of chemical species can also be used to characterize contrail/cirrus properties. The concentration depends strongly on the type of the tracked aircraft. Figure 6d shows the mean concentration of nitrogen oxide NO for the six individual clusters. Young contrail NO concentrations (cluster PW, YC1 and YC2) can reach values up to 10 nmol mol^{-1} (corresponding to 10% of measurements). For primary wake measurements (PW in black) a higher concentration can be reached. Approximately 1% of the data have concentrations close to 60 nmol mol^{-1} in the primary wake. In contrast, in aged contrails and in natural cirrus (cluster AC1, AC2 and CC) NO concentrations higher than 2 nmol mol^{-1} do not exceed 1% of cases. Indeed, after exhaust, concentrations of nitrogen oxide NO and sulphur dioxide SO2 created by combustion reactions decrease rapidly due to the dispersion in the upper troposphere and reactions with other molecules.

Finally, saturation conditions with respect to ice are presented in Fig. 6e for all clusters. The predominant measured ambient relative humidity of all clusters is around 95%. Cluster AC1 and CC (yellow and blue lines respectively) exhibit median RHI values close to 110% and 120% respectively. These higher values are suitable for the persistence of the contrail and the formation of cirrus clouds Supersaturated conditions are not reached for the measurements gathered in the primary wake cluster (PW). Low humidity values may well occur in primary wakes with non-persisting contrails.

These results highlight that the principal component analysis, based on the ASC measurements described in Sect. 3, can be used to discriminate contrail phases. Specific optical and chemical properties can thus be derived for each contrail phase and can be related to their evolution.

4.2 Microphysical cluster properties

Microphysical properties are assessed using the combination of FSSP-300 and 2DC measurements or hydrometeor diameters ranging from 0.5 µm to 800 µm, but with a gap in the size range 17 µm to 70 µm. Figure 7 shows the averaged number particle size distributions (PSD) for each cluster and for all flights of the study (8 flights from CONCERT-1 and 2). A linear interpolation in logarithmic space is applied for each PSD to cover the gap from 17 µm to 70 µm. Because of this gap, the derived microphysical properties should be considered with caution, but may be used to check the cluster definitions.

PSD measurements in natural cirrus and aged contrails differ significantly depending on the location of the study, ambient air conditions, measurement methods (instrument limitation (Gayet et al., 2002), and air speed (Febvre et al., 2009)). Previous studies show that a 3-hours old contrail cirrus with an effective diameter close to 20 µm (Voigt et al., 2017) and number concentration larger than 0.1cm^{-3} (Schumann et al., 2017) can be composed of ice crystals with sizes up to 100 µm (blue dashed line, contrail cirrus figure 7). This differs from the PSD of the natural cirrus presented by Voigt et al. (2017) (dashed black line), which has an order of magnitude lower particle number concentration. In natural cirrus at mid-latitudes, ice crystals with size up to 1600 µm were observed during the ML-CIRRUS campaign (dark dashed line Figure 7, Voigt et al., 2017).

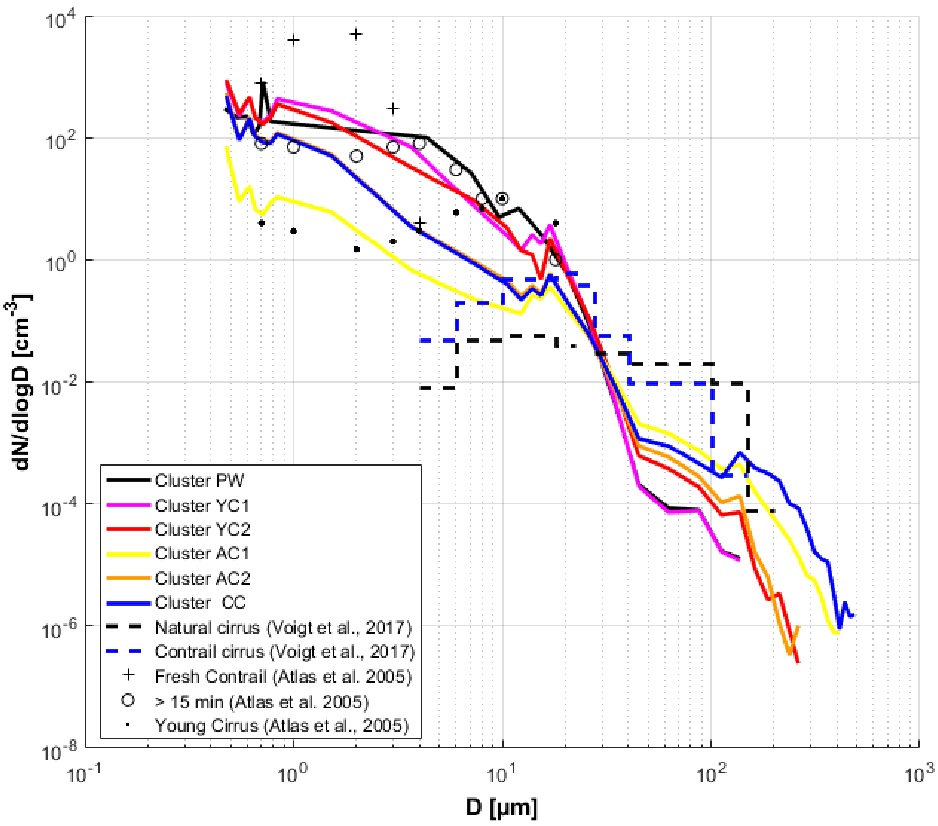

Figure 7: Number particle size distribution for each cluster including all data points of all flights. FSSP-300 measurements from 0.5 to 17 µm and 2DC measurements from 70 µm to 800 µm. The data are linearly interpolated in logarithm space between 17 µm and 70 µm.

Figure 7 shows that the mean number PSDs of each cluster are consistent with the cluster definition and these previous studies. Indeed, two categories of PSD can be observed. Within the FSSP-300 size range, PSD relative to old contrails (cluster AC1 and AC2) and cirrus (cluster CC) exhibit number concentration of small ice particles one order of magnitude lower than young contrails (clusters YC1 and YC2) and primary wake (cluster PW). Differences in this size range should be carefully considered due to uncertainties of the FSSP-300 number concentration measurements, which is close to 30% for typical concentrations of 5cm^{-3} but can reach 75% for concentrations of approximately 0.5 cm^{-3} (Gayet et al., 2002). However, we can still discriminate primary wake measurements (cluster PW) from secondary wake measurements (clusters YC1 and YC2) in the 3 to 10 µm size range. In addition, it is interesting to note that aged contrail measurements classified into AC1 cluster present significantly lower ice particle concentrations than natural cirrus. The differences observed between the PSD of PW/YC1/YC2 and AC1/AC2/CC can be explained by the production of small ice crystals (from 1 to 10 µm) in fresh exhaust plumes followed by rapid dilution during subsequent minutes after the exhaust.

Within the 2DC range, the PSDs are also in agreement with the cluster definitions. A higher concentration of large ice crystals with diameters around 100 µm and larger are expected for natural cirrus (cluster CC) and for significantly well-developed contrails. This is particularly well illustrated by the mean PSD from cluster YC1 that displays significantly less particles in the 2DC measurements size range than the one corresponding to AC1 and AC2.

Extinction (km^{-1})		Mean	std	Median	percentile 25	percentile 75
cluster	PW	4,230	3,820	3,308	1,104	6,485
	YC1	0,720	0,410	0,680	0,351	1,026
	YC2	2,070	2,655	1,017	0,271	2,836
	AC1	0,220	0,484	0,037	0,008	0,158
	AC2	0,110	0,161	0,054	0,004	0,126
	CC	0,370	1,240	0,046	0,001	0,132

IWC (mg m^{-3})		Mean	std	Median	percentile 25	percentile 75
cluster	PW	8,173	10,586	5,573	1,665	11,363
	YC1	0,191	0,107	0,168	0,111	0,281
	YC2	4,860	8,918	1,235	0,218	6,604
	AC1	7,072	35,765	0,124	0,000	1,151
	AC2	0,295	1,079	0,094	0,003	0,286
	CC	27,929	144,384	0,126	0,005	0,448

NTOTAL (cm^{-3})		Mean	std	Median	percentile 25	percentile 75
cluster	PW	172,965	114,497	152,398	95,564	223,374
	YC1	409,726	205,625	405,127	230,907	603,187
	YC2	188,139	199,736	125,344	52,584	236,100
	AC1	8,206	6,550	1,696	0,966	3,363
	AC2	28,883	43,758	9,176	2,954	42,626
	CC	5,092	24,453	3,444	1,467	6,511

Table 3: Optical and microphysical properties for each cluster according interpolated particle size distributions from FSSP-300 and 2DC measurements.

Table 3 presents ice water content (IWC, in mg m^{-3}) and total number of ice crystals (NTOTAL, in cm^{-3}) derived from the measured PSD for each cluster. The extinction coefficient (in km^{-1}) obtained from the PN measurements is also displayed. Despite the large uncertainties associated to both instruments and the interpolation between 17 µm and 70 µm diameters, these results again show that each cluster can be connected to a specific contrail phase, and their properties can be compared to previous studies.

In terms of cluster mean values, the microphysical and optical properties of cluster PW agree with the cloud properties expected in the primary wakes. The extinction coefficient has a mean value of 4.23 km^{-1}, IWC is close to 28 mg m^{-3}, and the number concentration yields a typical value of 173 particles cm^{-3}. These properties are in agreement with previous measurement reported by Gayet et al. (2012) with particle number concentrations close to 200 cm^{-3} for contrails less than 60 s after their formation. Their work also reports extinction coefficient around 7 km^{-1} presenting the highest values of the contrail life time.

Young (clusters YC1 and YC2) and aged contrails (clusters AC1 and AC2) exhibit distinctive differences in their extinction coefficients and their concentrations of ice particles. Higher extinction coefficients and ice number concentration, more than 0.7 km^{-1} and 170 cm^{-3}, respectively, characterize young contrails compared to aged contrails, with less than 0.4 km^{-1} and around 10 particles cm^{-3}, respectively. The ice number concentrations are in agreement with previous results with values between 200 and 100 cm^{-3} for contrail ages between 60 s and 3 min, and around 5 cm^{-3} for contrail ages around 10 min (Goodman et al., 1998 ; Lawson et al., 1998 ; Schröder et al., 2000 ; Schäuble et al., 2009 ; Gayet et al., 2012 ; Voigt et al., 2017). The IWC values differ significantly between clusters YC1 and YC2 which may be due to a lower number of large particles with diameter higher than 20 µm in YC1 than in YC2. Cluster CC corresponds to natural cirrus clouds which experienced strongly variable spreading and ice growth. Indeed, the

IWC is significantly higher (28 mg m^{-3}) within this cluster than in other clusters. However, the ice number concentration and the extinction coefficient are higher than in previous studies, with values around 0.1 cm^{-3} and 0.023 km^{-1} respectively. Besides to interpolation between the FSSP-300 and the 2DC measurements, the assumed shape (spherical or aspherical), and shattering of large ice particles in cirrus and aged contrails can also have a significant effect on the measurement of optical and microphysical properties (Gayet et al., 2012).

Conclusions

In this study, a new form of statistical analysis of contrail to cirrus evolution is presented based on two intensive contrail measurement campaigns, CONCERT-1 and CONCERT-2. The data are used to study optical and microphysical properties of contrails during their evolution from young contrails to contrail-cirrus clouds, and of ambient natural cirrus clouds. The combination of optical, microphysical, chemical airborne measurements with aircraft chasing information from ATC was used to provide an extended view of cloud properties.

A Principal Component Analysis (PCA) methodology was applied to the measured Polar Nephelometer scattering phase function data to facilitate the discrimination of cloud properties of different contrail phases. The PCA results were derived first for two reference flights that sampled contrails and cirrus in various development stages, including the primary wake, the young secondary wake, old contrails (few minutes after formation) and natural cirrus. For these flights, the PCA clearly demonstrates its potential to discriminate different groups of clouds, justifying the use of these two flights as a benchmark. Thereafter, the scattering phase functions measured during other CONCERT flights were projected into the space of principal components obtained from the two reference flights. Individual data points were assigned to the predefined cluster with minimum Mahalanobis distances. From the entire data set, the cloud properties in the various contrail development stages can be analysed separately.

The analysis demonstrates that the clearest separation between clusters is derived from particle shape, which impacts the scattering phase function and the derived asymmetry parameter gPN. The asymmetry parameter clearly separates young contrails (gPN of 0.72 to 0.80) from contrail/cirrus with gPN ranging from 0.80 to 0.88. Since the exact contrail age was not always known, young and aged contrails are classified also by their optical and chemical properties. The measured NO concentrations are also useful to distinguish natural cirrus from old contrails.

Despite the large size gap between the size ranges of the two instruments used, particle size spectra and related mean values of the ice particle number concentration, extinction and ice water content have been determined for each cluster. The various clusters clearly show different size distributions. In good agreement with previous findings on optical and chemical properties, we find that young contrails have more than a factor of ten higher number concentrations of small ice crystals (with diameters lower than 20 µm) than aged contrails and natural cirrus. On the other hand, aged contrails and natural cirrus contain larger ice crystals, with diameters larger than 75 µm. The optical and microphysical properties of the aged contrail cirrus are often similar to those found in the ambient “natural” cirrus clouds. The results show that the PCA method allows to identify and discriminate different contrail growth stages and to provide an independent method for the characterization of the evolution of contrail properties.

In agreement with Shcherbakov et al. (2016), who characterised volcanic and cirrus using optical measurements, the PCA method has been clearly shown here to be suitable for contrail studies. The additional use of microphysical and chemical measurements can be added to the PCA method in order to improve the selection of contrail phases. Different ranges of extinction or asymmetric coefficients could be also used for PCA analyses in this perspective. However, additional parameters should be carefully selected to limit the bias introduced by the limitations of the probes and the optimal selection may vary from one measurement campaign to another.

Accurate modelling of cirrus or contrails' single scattering properties is required for the interpretation of remote sensing measurements. Therefore, measurements of the optical characteristics of ice crystals in natural conditions are still needed for validation of numerical techniques and for the determination of free parameters in light scattering models. In this context, the results from the PCA could be used to develop representative parameterizations of the scattering properties and the ice crystals' shapes and sizes observed in the visible wavelength range.

Acknowledgments

We thank for financial support by the Helmholtz Association under contract VH-NG-309 and W2/W3-60. Part of this work was funded by DFG SPP HALO 1294 contract VO1504/4-1, and by the DLR project Eco2Fly in ML-CIRRUS-cirrus special issue. We thank Lufthansa, the DLR flight department and the Deutsche Flugsicherung for excellent support during the campaign. The in-situ data can be found in the HALO-database (https://halo-db.pa.op.dlr.de/).

References

Baran, A.J., Gayet, J.-F., and Shcherbakov, V.: On the interpretation of an unusual in-situ measured ice crystal scattering phase function. Atmospheric Chemistry and Physics 12, 9355–9364, 2012.

Baumgardner, D., Dye, J.E., Gandrud, B.W., and Knollenberg, R.G.: Interpretation of measurements made by the forward scattering spectrometer probe (FSSP-300) during the Airborne Arctic Stratospheric Expedition. Journal of Geophysical Research 97, 8035–8046, 1992.

Borrmann, S., Luo, B., and Mishchenko, M.; Application of the T-Matrix Method to the Measurement of Aspherical (Ellipsoidal) Particles with Forward Scattering Optical Particle Counters. Journal of Aerosol Science 31, no. 7 (2000): 789–799, 2000.

Burkhardt, U., Kärcher, B., and Schumann, U.: Global modeling of the contrail and contrail cirrus climate impact. Bulletin of the American Meteorological Society 91, 479–484, 2010.

Burkhardt, U. and Kärcher, B.: Global radiative forcing from contrail cirrus. Nature Climate Change, 1(1), 54–58, 2011.

Carleton, A.M., Silva, A.D., Aghazarian, M.S., Bernhardt, J., Travis, D.J., and Allard, J.: Mid-season climate diagnostics of jet contrail "outbreaks" and implications for eastern US sky-cover trends. Climate Research, 56, 209–230, 2013.

Chen, C.-C. and Gettelman, A.: Simulated 2050 aviation radiative forcing from contrails and aerosols. Atmospheric Chemistry and Physics, 16(11), 7317–7333, 2016.

Duda, D. P., Minnis, P., Khlopenkov, K., Chee, T.L., and Boeke, R.: Estimation of 2006 Northern Hemisphere Contrail Coverage Using MODIS Data. Geophysical Research Letters, 40, 612-617, doi:10.1002/grl.50097, 2013.

Febvre, G., Gayet, J.-F., Minikin, A., Schlager, H., Shcherbakov, V., Jourdan, O., Busen, R., Fiebig, M., Kärcher, B., and Schumann, U.: On optical and microphysical characteristics of contrails and cirrus. Journal of Geophysical Research: Atmospheres (1984–2012) 114, 2009.

Frömming, C., Ponater, M., Dahlmann, K., Grewe, V., Lee, D.S., and Sausen, R.: Aviation-induced radiative forcing and surface temperature change in dependency of the emission altitude. Journal of Geophysical Research: Atmospheres (1984–2012) 117, 2012.

Gayet, J.F., Crépel, O., Fournol, J.F., and Oshchepkov, S.: A new airborne Polar Nephelometer for the measurements of optical and microphysical cloud properties. Part I: Theoretical design. In Annales Geophysicae, pp. 451–459, 1997.

Gayet, J.-F., Auriol, F., Minikin, A., Ström, J., Seifert, M., Krejci, R., Petzold, A., Febvre, G., and Schumann, U.: Quantitative Measurement of the Microphysical and Optical Properties of Cirrus Clouds with Four Different in Situ Probes: Evidence of Small Ice Crystals. Geophysical Research Letters 29, no. 24: 2230. doi:10.1029/2001GL014342, 2002.

Gayet, J.-F., Ovarlez J., Shcherbakov, V., Ström, J., Schumann, U., Minikin, A., Auriol, F., Petzold, A., and Monier M.: Cirrus Cloud Microphysical and Optical Properties at Southern and Northern Midlatitudes during the INCA Experiment. Journal of Geophysical Research: Atmospheres 109, no. D20 : D20206. doi:10.1029/2004JD004803, 2004.

Gayet, J.-F., Shcherbakov, V., Voigt, C., Schumann, U., Schäuble, D., Jeßberger, P., Petzold, A., Minikin, A., Schlager, H., Dubovik, O., and Lapyonok, T.: The evolution of microphysical and optical properties of an A380 contrail in the vortex phase. Atmospheric Chemistry and Physics. 12, 6629–6643, 2012.

Garrett, T.J., Gerber, H., Baumgardner, D.G., Twohy, C.H., and Weinstock, E.M.: Small, highly reflective ice crystals in low-latitude cirrus. Geophysical Research Letters 30, 2132, 2003.

Gettelman, A., and Chen, C.: The climate impact of aviation aerosols. Geophysical Research Letters, 40, 2785–2789, doi:10.1002/grl.50520, 2013.

Gierens, K. and Dilger, F.: A climatology of formation conditions for aerodynamic contrails, Atmospheric Chemistry and Physics, 13, 10847-10857, doi:10.5194/acp-13-10847-2013, 2013.

Graf, K., Schumann, U., Mannstein, H., and Mayer, B.: Aviation induced diurnal North Atlantic cirrus cover cycle. Geophysical Research Letters 39, L16804, doi:10.1029/2012GL052590, 2012.

Goodman, J., Pueschel, R.F., Jensen, E.J., Verma, S., Ferry, G.V., Howard, S.D., Kinne, S.A., and Baumgardner, D.: Shape and size of contrails ice particles. Geophysical Research Letters 25, 1327–1330, 1998.

Heller, R., Voigt, C., Beaton, S., Dörnbrack, A., Kaufmann, S., Schlager, H., Wagner, J., Young, K., and Rapp, M.: Mountain waves modulate the water vapor distribution in the UTLS, Atmospheric Chemistry and Physics, Discussion, doi:10.5194/acp-2017-334, in review.

Heymsfield, A.J., and Parrish, J.L.: A computational technique for increasing the effective sampling volume of the PMS two-dimensional particle size spectrometer. Journal of Applied Meteorology 17, 1566–1572, 1978.

Heymsfield, A., Baumgardner, D., DeMott, P., Forster, P., Gierens, K., and Kärcher, B.: Contrail Microphysics. Bulletin of the American Meteorological Society 91, 465–472, 2010.

Irvine, E.A., Hoskins, B.J., and Shine, K.P.: The dependence of contrail formation on the weather pattern and altitude in the North Atlantic. Geophysical Research Letters 39, L12802, doi:10.1029/2012GL051909, 2012.

Järvinen, E., Schnaiter, M., Mioche, G., Jourdan, O., Shcherbakov, V.N., Costa, A., Afchine, A., Krämer, M., Heidelberg, F., Jurkat, T., Voigt, C., Schlager, H., Nichman, L., Gallagher, M., Hirst, E., Schmitt, C., Bansemer, A., Heymsfield, A., Lawson, P., Tricoli, U., Pfeilsticker, K., Vochezer, P., Möhler, O., and Leisner, T.: Quasi-spherical Ice in Convective Clouds, Journal of Atmospheric Sciences, doi:10.1175/JAS-D-15-0365.1, 2016.

Jansen, J. and Heymsfield, A. J.: Microphysics of aerodynamic contrail formation processes, Journal of Atmospheric Sciences, 72(9), 3293–3308, 2015.

Jeßberger, P., Voigt, C., Schumann, U., Sölch, I., Schlager, H., Kaufmann, S., Petzold, A., Schäuble, D., and Gayet, J.F.: Aircraft type influence on contrail properties, Atmospheric Chemistry and Physics, 13, 11965-11984, doi:10.5194/acp-13-11965-2013, 2013.

Jourdan, O., Oshchepkov, S., Gayet, J.-F., Shcherbakov, V., and Isaka, H.: Statistical analysis of cloud light scattering and microphysical properties obtained from airborne measurements. Journal of Geophysical Research 108, 4155, 2003.

Jourdan, O., Mioche, G., Garrett, T.J., Schwarzenböck, A., Vidot, J., Xie, Y., Shcherbakov, V., Yang, P., and Gayet, J.-F.: Coupling of the microphysical and optical properties of an Arctic nimbostratus cloud during the ASTAR 2004 experiment: Implications for light-scattering modeling. Journal of Geophysical Research: Atmospheres (1984–2012) 115, 2010.

Jurkat, T., Voigt, C., Arnold, F., Schlager, H., Aufmhoff, H., Schmale, J., Schneider, J., Lichtenstern, M., and Dörnbrack, A.: Airborne stratospheric ITCIMS-measurements of SO_2, HCl, and HNO_3 in the aged plume of volcano Kasatochi, Journal of Geophysical Research, 115, D00L17, doi:10.1029/2010JD013890, 2010.

Jurkat, T., Voigt, C., Arnold, F., Schlager, H., Kleffmann, J., Aufmhoff, H., Schäuble, D., Schäfer, M., and Schumann, U.: Measurements of HONO, NO, NOy and SO2 in aircraft exhaust plumes at cruise, Geophysical Research Letters, 38, L10807, doi:10.1029/2011GL046884, 2011.

Jurkat, T., Kaufmann, S., Voigt, C., Schäuble, D., Jeßberger, P., and Ziereis, H.: The airborne mass spectrometer AIMS – Part 2: Measurements of trace gases with stratospheric or tropospheric origin in the UTLS, Atmospheric Measurement Technics, 9, 1907–1923, doi:10.5194/amt-9-1907-2016, 2016.

Kärcher, B., and Voigt, C.: Formation of nitric acid/water ice particles in cirrus clouds, Geophysical Research Letters, 33, L08806, doi:10.1029/ 2006GL025927, 2006.

Kärcher, B., and Voigt, C.: Susceptibility of contrail ice crystal numbers to aircraft soot particle emissions, Geophysical Research Letters, 44, 8037-8046, doi:10.1002/2017GL074949, 2017.

Kärcher, B., and Yu, F.: Role of aircraft soot emissions in contrail formation. Geophysical Research Letters, 36, L01804, doi:10.1029/2008GL036649, 2009.

Kaufmann, S., Voigt, C., Jeßberger, P., Jurkat, T., Schlager, H., Schwarzenboeck, A., Klingebiel, M., and Thornberry, T.: In situ measurements of ice saturation in young contrails, Geophysical Research Letters, 41, doi:10.1002/2013GL058276, 2014.

Kaufmann, S., Voigt, C., Jurkat, T., Thornberry, T., Fahey, D. W., Gao, R.-S., Schlage, R., Schäuble, D., and Zöger, M.: The airborne mass spectrometer AIMS – Part 1: AIMS-H_2O for UTLS water vapor measurements, Atmospheric Measurement Technics, 9, 939-953, doi:10.5194/amt-9-939-2016, 2016.

Kübbeler, M., Hildebrandt, M., Meyer, J., Schiller, C., Hamburger, Th., Jurkat, T., Minikin, A., Petzold, A., Rautenhaus, M., Schlager, H., Schumann, U., Voigt, C., Spichtinger, P., Gayet, J.-F., Gourbeyre, C., and Krämer, M.: Thin and subvisible cirrus and contrails in a subsaturated environment, Atmospheric Chemistry and Physics, 11, 5853-5865, doi:10.5194/acp-11-5853-2011, 2011.

Lawson, R. Paul, Andrew J. Heymsfield, Steven M. Aulenbach, et Tara L. Jensen. « Shapes, sizes and light scattering properties of ice crystals in cirrus and a persistent contrail during SUCCESS ». Geophysical research letters 25, no 9: 1331–1334, 1998.

Lawson, R.P., O'Connor, D., Zmarzly, P., Weaver, K., Baker, B., Mo, Q., and Jonsson, H.: The 2D-S (stereo) probe: Design and preliminary tests of a new airborne, high-speed, high-resolution particle imaging probe. Journal of Atmospheric and Oceanic Technology 23, 1462–1477, 2006.

Lee, D.S., Pitari, G., Grewe, V., Gierens, K., Penner, J.E., Petzold, A., Prather, M.J., Schumann, U., Bais, A., and Berntsen, T.: Transport impacts on atmosphere and climate: Aviation. Atmospheric Environment 44, 4678–4734, 2010.

Legendre, P., and Legendre, L.: Numerical Ecology, 2nd English ed., 853 pp., Elsevier Science, New York, 1998.

De León, R.R., Krämer, M., Lee, D.S., and Thelen, J.C.: Sensitivity of radiative properties of persistent contrails to the ice water path. Atmospheric Chemistry and Physics. 12, 7893–7901, 2012.

Lewellen, D.C.: Analytic solutions for evolving size distributions of spherical crystals or droplets undergoing diffusional growth in different regimes. Journal of the Atmospheric Sciences 69, 417–434, 2012.

Lewellen, D.C., and Lewellen, W.S.: The effects of aircraft wake dynamics on contrail development. Journal of the Atmospheric Sciences 58, 390–406, 2001.

Liou, K.N., Takano, Y., Yue, Q., and Yang, P.: On the radiative forcing of contrail cirrus contaminated by black carbon. Geophysical Research Letters, 40, 778–784, doi:10.1002/grl.50110, 2013.

De Maesschalck, R., Jouan-Rimbaud, D., and Massart, D.L.: The Mahalanobis Distance. Chemometrics and Intelligent Laboratory Systems 50, no. 1: 1–18. doi:10.1016/S0169-7439(99)00047-7, 2010.

Meyer, J., Rolf, C., Schiller, C., Rohs, S., Spelten, N., Afchine, A., Zöger, M., Sitnikov, N., Thornberry, T. D., Rollins, A. W., Bozóki, Z., Tátrai, D., Ebert, V., Kühnreich, B., Mackrodt, P., Möhler, O., Saathoff, H., Rosenlof, K. H., and Krämer, M.: Two decades of water vapor measurements with the FISH fluorescence hygrometer: a review, Atmospheric Chemistry and Physics, 15, 8521–8538, doi:10.5194/acp-15-8521-2015, 2015.

Mishchenko, M.I., Travis, L.D., Kahn, R.A., and West, R.A.: Modeling phase functions for dustlike tropospheric aerosols using a shape mixture of randomly oriented polydisperse spheroids. Journal of Geophysical Research 102, 16831–16, 1997.

Moore, R. H., Thornhill, K. L., Weinzierl, B., Sauer, D., D'Ascoli, E., Kim, J., Lichtenstern, M., Scheibe, M., Beaton, B., Beyersdorf, A. J., Barrick, J., Bulzan, D., Corr, C. A., Crosbie, E., Jurkat, T., Martin, R., Riddick, D., Shook, M., Slover, G., Voigt, C., White, R., Winstead, E., Yasky, R., Ziemba, L. D., Brown, A., Schlager, H., and Anderson, B. E.: Biofuel blending reduces particle emissions from aircraft engines at cruise conditions, Nature, 543, 411-415, 10.1038/nature21420, 2017.

Schäuble, D., Voigt, C., Kärcher, B., Stock, P., Schlager, H., Krämer, M., Schiller, C., Bauer, R., Spelten, N., De Reus, M.., Szakáll, M., Borrmann, S., Weers, U., and Peter T.: Airborne measurements of the nitric acid partitioning in persistent contrails, Atmospheric Chemistry and Physics, 9, 8189-8197, 2009.

Schlager, H., Konopka, P., Schulte, P., Schumann, U., Ziereis, H., Arnold, F., Klemm, M., Hagen, D.E., Whitefield, P.D., and Ovarlez, J.: In situ observations of air traffic emission signatures in the North Atlantic flight corridor. Journal of Geophysical Research 102, 10739–10, 1997.

Schröder, F., Kärcher, B., Duroure, C., Ström, J., Petzold, A., Gayet, J.-F., Strauss, B., Wendling, P., and Borrmann, S.: On the Transition of Contrails into Cirrus Clouds. Journal of the Atmospheric Sciences 57, 464–480, 2000.

Schumann, U.: On conditions for contrail formation from aircraft exhausts. Meteorologische Zeitschrift, 5, 4–23, 1996.

Schumann, U., and Heymsfield, A.: On the lifecycle of individual contrails and contrail cirrus, Meteorological Monographs, 58, 3.1-3.24, doi: 10.1175/AMSMONOGRAPHS-D-16-0005.1, 2017.

Schumann, U., Jeßberger, P., and Voigt, C.: Contrail ice particles in aircraft wakes and their climatic importance, Geophysical Research Letters, 40, 2867-2872, doi: 10.1002/grl.50539, 2013.

Schumann, U., Mayer, B., Gierens, K., Unterstrasser, S., Jessberger, P., Petzold, A., Voigt, C., and Gayet, J.-F.: Effective Radius of Ice Particles in Cirrus and Contrails. Journal of the Atmospheric Sciences, 68, 300–321, 2011.

Schumann, U., Penner, J.E., Chen, Y., Zhou, C., and Graf, K.: Dehydration effects from contrails in a coupled contrail-climate model, Atmospheric Chemistry and Physics, 15, 11179-11199, doi: 10.5194/acp-15-11179-2015, 2015.

Schumann, U., Kiemle, C., Schlager, H., Weigel, R., Borrmann, S., D'Amato, F., Krämer, M., Matthey, R., Protat, A., Voigt, C., and Volk, C. M.: Long-lived contrails and convective cirrus above the tropical tropopause, Atmospheric Chemistry and Physics, 17, 2311-2346, doi:10.5194/acp-17-2311-2017, 2017a.

Schumann, U., Baumann, R., Baumgardner, D., Bedka, S. T., Duda, D. P., Freudenthaler, V., Gayet, J.-F., Heymsfield, A. J., Minnis, P., Quante, M., Raschke, E., Schlager, H., Vázquez-Navarro, M., Voigt, C. and Wang, Z.: Properties of individual contrails: a compilation of observations and some comparisons, Atmospheric Chemistry and Physics, 17(1), 403–438, doi:10.5194/acp-17-403-2017, 2017b.

Seber, G. A. F.: Multivariate analysis of variance and covariance. Multivariate observations, 433–495, 1984.

Shcherbakov, V., Jourdan, O., Voigt, C., Gayet, J.F., Chauvigne, A., Schwarzenboeck, A., Minikin, A., Klingebiel, M., Weigel, R., Borrmann, S., Jurkat, T., Kaufmann, S., Schlage, R., Gourbeyre, C., Febvre, G., Lapyonok, T., Frey, W., Molleker, S., and Weinzierl, B.: Porous Aerosol in Degassing Plumes of Mt. Etna and Mt. Stromboli. Atmospheric Chemistry Physics 16, no. 18: 11883–97. doi:10.5194/acp-16-11883-2016, 2016.

Spath, Helmuth. The Cluster Dissection and Analysis Theory FORTRAN Programs Examples. Prentice-Hall, Inc., 1985.

Sussmann, R., and Gierens, K.M.: Lidar and numerical studies on the different evolution of vortex pair and secondary wake in young contrails. Journal of Geophysical Research: Atmospheres 104, 2131–2142, 1999.

Sussmann, R., and Gierens, K.M.: Differences in early contrail evolution of two-engine versus four-engine aircraft: Lidar measurements and numerical simulations. Journal of Geophysical Research: Atmospheres 106, 4899–4911, 2001.

Vazquez-Navarro, M., Mannstein, H. and Kox, S.: Contrail life cycle and properties from 1 year of MSG/SEVIRI rapid-scan images, Atmospheric Chemistry and Physics, 15(15), 8739–8749, 2015.

Voigt C., Schlager, H., Ziereis, H., Kärcher, B., Luo, B.P., Schiller, C., Krämer, M., Popp, P.J., Irie, H., and Kondo, Y.: Nitric acid in cirrus clouds, Geophysical Research Letters, 33, L05803, doi:10.1029/2005GL025159, 2006.

Voigt, C., Schumann, U., Jurkat, T., Schäuble, D., Schlager, H., Petzold, A., Gayet, J.-F., Krämer, M., Schneider, J., Borrmann, S., Schmale, J., Jessberger, P., Hamburger, T., Lichtenstern, M., Scheibe, M., Gourbeyre, C., Meyer, J., Kübbeler, M., Frey, W., Kalesse, H., Butler, T., Lawrence, M.G., Holzäpfel. F., Arnold, F., Wendisch, M., Döpelheuer, A., Gottschaldt, K., Baumann, R., Zöger, M., Sölch, I., Rautenhaus, M., and Dörnbrack, A.: In-situ observations of young contrails - Overview and selected case studies from the CONCERT campaign, Atmospheric Chemistry and Physics, 10, 9039–9056, doi:10.5194/acp-10-9039-2010, 2010.

Voigt, C., Schumann, U., Jessberger, P., Jurkat, T., Petzold, A., Gayet, J.-F., Krämer, M., Thornberry, T., and Fahey, D.: Extinction and optical depth of contrails, Geophysical Research Letters, 38, L11806, doi:10.1029/2011GL04718, 2011.

Voigt, C., Jessberger, P., Jurkat, T., Kaufmann, S., Baumann, R., Schlager, H., Bobrowski, N., Giuffrida, G., and Salerno, G.: Evolution of CO_2, SO_2, HCl, and HNO_3 in the Volcanic Plumes from Etna. Geophysical Research Letters, 41, 6, 2196-2203. doi:10.1002/2013GL058974, 2014.

Voigt, C., Schumann, U., Minikin, A., Abdelmonem, A., Afchine, A., Borrmann, S., Boettcher, M., Buchholz, B., Bugliaro, L., Costa, A., Curtius, J., Dollner, M., Dörnbrack, A., Dreiling, V., Ebert, V., Ehrlich, A., Fix, A., Forster, L., Frank, F., Fütterer, D., Giez, A., Graf, K., Grooß, J.-U., Groß, S., Heimerl, K., Heinold, B., Hüneke, T., Järvinen, E., Jurkat, T., Kaufmann, S., Kenntner, M., Klingebiel, M., Klimach, T., Kohl, R., Krämer, M., Krisna, T. C., Luebke, A., Mayer, B., Mertes, S., Molleker, S., Petzold, A., Pfeilsticker, K., Port, M., Rapp, M., Reutter, P., Rolf, C., Rose, D., Sauer, D., Schäfler, A., Schlage, R., Schnaiter, M., Schneider, J., Spelten, N., Spichtinger, P., Stock, P., Walser, A., Weigel, R., Weinzierl, B., Wendisch, M., Werner, F., Wernli, H., Wirth, M., Zahn, A., Ziereis, H., and Zöger, M.: ML-CIRRUS - The airborne experiment on natural cirrus and contrail cirrus with the high-altitude long-range research aircraft HALO, Bulletin of the American Meteorological Society, doi: 10.1175/BAMS-D-15-00213, 2017.

Xie, Y., Yang, P., Gao, B.-C., Kattawar, G.W., and Mishchenko, M.I.: Effect of ice crystal shape and effective size on snow bidirectional reflectance. Journal of Quantitative Spectroscopy and Radiative Transfer 100, 457–469, 2006.

Xie, Y., Yang, P., Kattawar, G.W., Minnis, P., and Hu, Y.X.: Effect of the inhomogeneity of ice crystals on retrieving ice cloud optical thickness and effective particle size. Journal of Geophysical Research: Atmospheres (1984–2012) 114, 2009.

Yang, P., Hong, G., Dessler, A.E., Ou, S.S., Liou, K.-N., and Minnis, P.: Contrails and induced cirrus: Optics and radiation. Bulletin of the American Meteorological Society 91, 473–478, 2010.

Ziereis, H., Schlager, H., Schulte, P., Velthoven, P. van, and Slemr, F.: Distributions of NO, NO_x, and NO_y in the upper troposphere and lower stratosphere between 28 and 61 N during POLINAT 2. Journal of Geophysical Research: Atmospheres (1984–2012) 105, 3653–3664, 2000.

Zöger, M., Afchine, A., Eicke, N., Gerhards, M-T., Klein, E., McKenna, D.S., Mörschel, U., Schmidt, U., Tan, V., Tuitjer, F., Woyke, T., Schiller, C. : Fast in situ stratospheric hygrometers: A new family of balloon-borne and airborne Lyman alpha photofragment fluorescence hygrometers. Journal of Geophysical Research: Atmospheres, 104, 1807-1816, 1999.